Spin-Forbidden Transitions in the Vicinity of the 2 $^1\Pi_u \leftarrow$ X $^1\Sigma_g^+$ Band System of Rb_2

Yonghoon Lee,[†] Sungyul Lee,[‡] and Bongsoo Kim*[,§]

Advanced Photonics Research Institute, Gwangju Institute of Science and Technology, Gwangju 500-712, Korea, College of Environmental Science and Applied Chemistry (BK21), Kyunghee University, Kyungki-do 449-701, Korea, and Department of Chemistry, KAIST, Daejeon 305-701, Korea

Received: February 21, 2008; Revised Manuscript Received: April 29, 2008

We have investigated the Rb_2 475 nm system by resonance enhanced two-photon ionization spectroscopy in a pulsed molecular beam. Strong extra bands accompanying the 2 $^1\Pi_u$ $v' = 5 - 8 \leftarrow$ X $^1\Sigma_g^+$ $v'' = 0$ bands were newly observed. Rotational analysis of the main and extra bands reveals that the 2 $^1\Pi_u$ $v' = 5 - 8$ levels are significantly perturbed, mainly by the 3 $^3\Sigma_u^+(1_u)$ state and also by the 2 $^3\Pi_u(1_u)$ state. For the major perturber, 3 $^3\Sigma_u^+(1_u)$, the intensity borrowing has been found to be facilitated by the 2 $^1\Pi_u$−3 $^3\Sigma_u^+(1_u)$ potential energy curve crossing near 21100 cm^{-1}. For the vibronic-band intensities of the 2 $^3\Pi_u(1_u)$ $v' \leftarrow$ X $^1\Sigma_g^+$ $v'' = 0$ transitions observed in this spectral region, intensity borrowing was most effective when the 2 $^3\Pi_u(1_u)$ levels were close to the 3 $^3\Sigma_u^+(1_u)$ levels. A deperturbation fit for the perturbing bands has provided the 2 $^1\Pi_u$−3 $^3\Sigma_u^+(1_u)$ coupling constants.

1. Introduction

Diatomic rubidium, Rb_2, one of the heavy homonuclear alkali metal diatomic molecules, has provided superb systems for molecular spectroscopy,[1–8] photodissociation dynamics,[8–11] photoassociation spectroscopy,[12,13] and theoretical study of the electronic states.[14–17] For the ground and several excited electronic states below the Rb(5s) + Rb(5p) atomic limit (X $^1\Sigma_g^+$, 2 $^1\Sigma_g^+$, 1 $^1\Pi_u$, and 1 $^1\Pi_g$), potential energy curves have been experimentally determined.[1–4] For the higher-lying excited electronic states, Tsi-Zé and San-Tsiang observed the 2 $^1\Pi_u$ state near 475 nm and the 3 $^1\Pi_u$ state near 430 nm by measuring molecular fluorescence in a high-temperature steel tube.[5] These two $^1\Pi_u$ states have been known as C and D states, respectively. Subsequently, predissociation of the 475 and 430 nm systems have been identified by several groups.[8–11] For the 2 $^1\Pi_u$ state in the 475 nm system, Dunham coefficients and Rydberg−Klein−Rees (RKR) potential energy curve were obtained using high-resolution Fourier-transform (FT) spectroscopy in a heat pipe oven.[4] However, identification of the higher-lying excited electronic states of heavy alkali metal diatomic molecules is quite challenging because the number of nearby electronic states increases greatly, making perturbations due to spin−orbit coupling more prevalent as the excitation energy is increased. Under these circumstances, resonance enhanced multiphoton ionization in a very cold molecular beam combined with mass spectrometric detection can be a useful approach for identifying the congested electronically excited states, which overlap and perturb each other. The mass-resolved spectrum obtained by this approach can be greatly simplified by vibrational and rotational cooling and the observed isotope shifts provide valuable information for the assignment of vibrational quantum numbers.[8] Recently, mass-resolved resonance enhanced two-photon ionization (RE2PI) of Rb_2 in a pulsed molecular beam has identified the 1 $^1\Delta_g \leftarrow$ X $^1\Sigma_g^+$ electric quadrupole transition near 540 nm,[7] the 2 $^3\Pi_u \leftarrow$ X $^1\Sigma_g^+$ triplet−singlet transition near 500 nm,[6] and the 3 $^1\Pi_u$, 3 $^1\Sigma_u^+$, 3 $^3\Pi_u(1_u, 0_u^+) \leftarrow$ X $^1\Sigma_g^+$ transitions and the predissociation channels near 430 nm.[8]

In this work, we report the RE2PI study of the Rb_2 475 nm system in a pulsed molecular beam. The strongest 2 $^1\Pi_u \leftarrow$ X $^1\Sigma_g^+$ transition is accompanied by several extra bands in our RE2PI spectrum. Through the rotational analysis of the main and extra bands, the 3 $^3\Sigma_u^+(1_u)$ and 2 $^3\Pi_u(1_u)$ states have been assigned to the upper electronic states of the extra bands. The 2 $^1\Pi_u$ $v' = 5-8$ levels have been found to be significantly perturbed by the 3 $^3\Sigma_u^+(1_u)$ state. Isotope shifts of the extra bands between $^{85}Rb_2$ and $^{85}Rb^{87}Rb$ are consistent with these assignments. For the detailed intensity borrowing mechanisms of the 3 $^3\Sigma_u^+(1_u)$ and 2 $^3\Pi_u(1_u)$ states, the 2 $^1\Pi_u$−3 $^3\Sigma_u^+(1_u)$ potential energy curve crossing and the energy-level proximity effect of 3 $^3\Sigma_u^+(1_u)$−2 $^3\Pi_u(1_u)$ have been suggested, respectively. From a deperturbation fit of the perturbing bands, the 2 $^1\Pi_u$−3 $^3\Sigma_u^+(1_u)$ coupling constant has been estimated.

2. Experiment

Our experimental apparatus and techniques have been discussed previously.[6] Briefly, we prepared Rb_2 by expanding Rb vapor with Ar gas (stagnation pressure, 760 Torr) through a high-temperature pulsed nozzle. The temperature of the nozzle was maintained at 330 °C in this experiment. The nozzle diameter was 800 μm. The pulsed jet was collimated by a skimmer with a 1.2 mm diameter, located 7 cm from the nozzle. Rb_2^+ ions were generated by the absorption of two photons from a dye laser (Lambda Physik Scanmate 2E) pumped by the third harmonic of a Nd:YAG laser (Spectra Physics GCR-150). Three different isotopomers of Rb_2 ($^{85}Rb_2$, 52.1%; $^{85}Rb^{87}Rb$, 40.2%; $^{87}Rb_2$, 7.8%) were well separated and detected by a linear time-of-flight (TOF) mass spectrometer ($m/\Delta m \sim 500$). Low-resolution RE2PI spectra were obtained with 0.12 cm^{-1} laser line width. To record rotationally resolved RE2PI spectra, we installed an intracavity étalon that narrowed the laser line width to 0.02 cm^{-1}. The wavelength of the dye laser was calibrated by a wavemeter (Burleigh WA-4500) and Ne optogalvanic spectrum for the low-resolution scan. For the wavelength

* To whom correspondence should be addressed. E-mail: bongsoo@kaist.ac.kr. Fax: +82-42-869-2810.
† Advanced Photonics Research Institute.
‡ Kyunghee University.
§ KAIST.

10.1021/jp801560a CCC: $40.75
Published on Web 07/09/2008

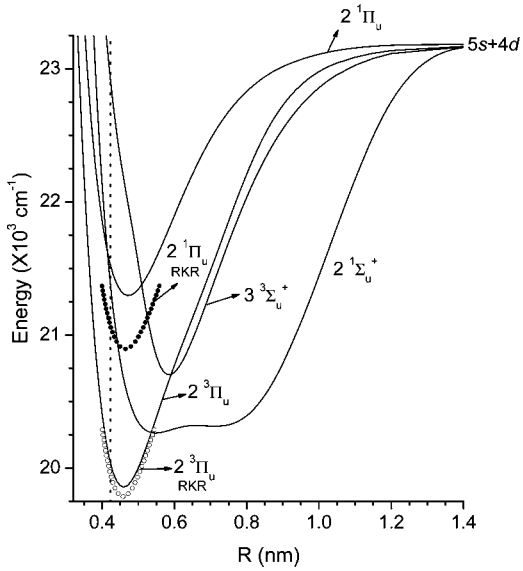

Figure 1. Ab initio potential energy curves of Rb_2 for the 2 $^1\Pi_u$, 2 $^1\Sigma_u^+$, 2 $^3\Pi_u$, and 3 $^3\Sigma_u^+$ states from ref 16 and RKR curves of the 2 $^1\Pi_u$ and 2 $^3\Pi_u$ states generated from the molecular constants reported in refs 4 and 6, respectively.

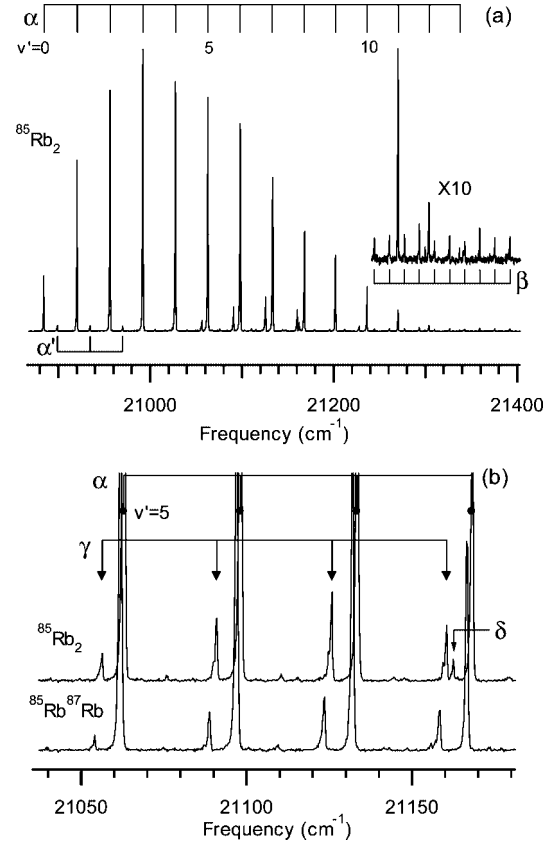

Figure 2. Low-resolution RE2PI spectrum of (a) $^{85}Rb_2$ and (b) $^{85}Rb_2$ and $^{85}Rb^{87}Rb$ expanded in the region where the extra bands are observed strongly near the α $v' = 5-8$ bands.

calibration of the high-resolution scans, an I_2 laser-induced fluorescence (LIF) spectrum[18] was obtained using the Raman shifted beam (the first Stokes line) of a part of the dye laser using the high-pressure H_2 cell. The Raman shift was determined to be 4155.226 ± 0.002 cm^{-1} when the pressure of the H_2 gas in the Raman cell was kept constant at about 11.2 atm during the experiment.[19]

3. Results and Discussion

3.1. Overview of the Rb_2 475 nm System. Figure 1 shows the ab initio potential energy curves of Rb_2 for the 2 $^1\Pi_u$, 2 $^1\Sigma_u^+$, 2 $^3\Pi_u$, and 3 $^3\Sigma_u^+$ states,[16] and RKR potential energy curves of the 2 $^1\Pi_u$ and 2 $^3\Pi_u$ states generated from the molecular constants previously reported.[4,6] Around 21000 cm^{-1}, the inner potential walls of the singlet excited states (2 $^1\Pi_u$ and 2 $^1\Sigma_u^+$) are located in the Franck−Condon region (see the vertical dotted line in Figure 1) and the triplet excited states (3 $^3\Sigma_u^+$ and 2 $^3\Pi_u$) overlap the singlet states. Through vertical transitions from the X $^1\Sigma_g^+$ $v'' = 0$ level, the two singlet states (2 $^1\Pi_u$ and 2 $^1\Sigma_u^+$) are accessible; these are termed the "Franck−Condon bright states". Even allowing spin−orbit coupling, however, the two triplet states (3 $^3\Sigma_u^+$ and 2 $^3\Pi_u$) are inaccessible because of very poor Franck−Condon factors; these are termed the "Franck−Condon dark states".[20] Among the four excited electronic states near 475 nm, only the 2 $^1\Pi_u$ state has been observed so far.[4]

Figure 2 shows the mass-resolved low-resolution RE2PI spectra of $^{85}Rb_2$ and $^{85}Rb^{87}Rb$ isotopomers. The low-resolution spectrum of $^{85}Rb_2$ between 20860 and 21400 cm^{-1} and the expanded spectra of $^{85}Rb_2$ and $^{85}Rb^{87}Rb$ between 21040 and 21180 cm^{-1} are shown in Figure 2a,b, respectively. The strongest transitions, indicated as progression α in Figure 2a, are straightforwardly assigned to the 2 $^1\Pi_u$ $v' = 0-13 \leftarrow$ X $^1\Sigma_g^+$ $v'' = 0$ band system. The vibronic band positions of the 2 $^1\Pi_u$ state derived from the Dunham coefficients reported in ref 4 are indicated by the sticks of the α progression in Figure 2a. The vibrationally hot bands, 2 $^1\Pi_u$ $v' = 2-4 \leftarrow$ X $^1\Sigma_g^+$ $v'' = 1$, indicated as the α' progression in Figure 2a, confirm the initial level of the observed transitions (X $^1\Sigma_g^+$ $v'' = 0$). The observed differences between the cold and hot bands (57.6, 57.5, and 57.6 cm^{-1} for $v' = 2$, 3, and 4) agree well with $\Delta G_{v''=0} = G_{v''=1} - G_{v''=0}$ from high-resolution FT spectroscopy (57.5088 cm^{-1}).[1] The β progression, which is much weaker in intensity than the α progression, can be assigned to the 2 $^1\Sigma_u^+ \leftarrow$ X $^1\Sigma_g^+$ transition. The relatively small vibrational spacing ($\sim$16 cm^{-1}) is characteristic of the broad potential well that exists due to the interaction with the ionic potential in alkali metal diatomic molecules. The rotational structure of the β bands, consisting of *P*- and *R*-branch rotational lines, leads to the assignment of the upper electronic state as the 2 $^1\Sigma_u^+$ state (see the Supporting Information). The most remarkable feature observed in our RE2PI spectrum is the clear appearance of the extra bands, as shown in Figure 2b. The 2 $^1\Pi_u$ ($v' = 5-8$) $\leftarrow$ X $^1\Sigma_g^+$ ($v'' = 0$) bands of $^{85}Rb_2$ and $^{85}Rb^{87}Rb$ are accompanied by several extra bands indicated as γ and δ in Figure 2b. Our discussion is focused on the assignment of the extra bands and their intensity borrowing mechanisms.

3.2. Perturbation of the 2 $^1\Pi_u$ State. Amiot reported Dunham coefficients and a RKR potential energy curve of the 2 $^1\Pi_u$ states as well as those of the 1 $^1\Sigma_g^+$, 2 $^1\Sigma_g^+$, 1 $^1\Pi_u$, 1 $^1\Pi_g$, and X $^1\Sigma_g^+$ states.[4] In this previous work, much larger root-mean-square errors of the Dunham fits for the 1 $^1\Pi_u$ and 2 $^1\Pi_u$ states were noted (a factor of 20−30 times larger), in comparison to the other states. This provides a hint of the existence of perturbations in the 1 $^1\Pi_u$ and 2 $^1\Pi_u$ states due to dark states that cannot be directly observed. However, the perturbation of the 2 $^1\Pi_u$ state has not been identified yet. In the case of a homogeneous perturbation ($\Delta\Omega = 0$ with $\Delta J = 0$), where the interaction matrix element is independent of the rotational quantum number, *J*,[21] the molecular band parameters (band origin, ν_0, and rotational constant, B_v) obtained by fitting each vibronic band reveal more explicitly the effect of perturba-

TABLE 1: Effective Band Parameters of α Progression (Units in cm^{-1})

	$^{85}Rb_2$			$^{85}Rb^{87}Rb$		
$v' - v''$	ν_0	$10^2 B_{v'}^{\text{eff}}$	$10^8 D_{v'}$ [a]	ν_0	$10^2 B_{v'}^{\text{eff}}$	$10^8 D_{v'}$ [a]
0−0	20884.2838(13)	1.83729(23)	1.7959	20884.3446(12)	1.81580(20)	1.7548
1−0	20920.5386(16)	1.83025(43)	1.8037	20920.3862(23)	1.8093(16)	1.7624
2−0	20956.5419(14)	1.82290(61)	1.8115	20956.1942(16)	1.80299(47)	1.7700
3−0	20992.3114(14)	1.81605(34)	1.8193	20991.7581(11)	1.79561(42)	1.7776
4−0	21027.8322(23)	1.80630(47)	1.8271	21027.0673(26)	1.78939(69)	1.7852
5−0	21063.1323(14)	1.79742(28)	1.8349	21062.1706(13)	1.77739(34)	1.7927
6−0	21098.3980(21)	1.77562(39)	1.8427	21097.1976(13)	1.75781(31)	1.8003
7−0	21133.6951(39)	1.75400(72)	1.8505	21132.2782(22)	1.73582(53)	1.8079
8−0	21168.3963(20)	1.75417(53)	1.8583	21166.8382(12)	1.73517(48)	1.8155
9−0	21202.2474(9)	1.77144(30)	1.8661	21200.5475(15)	1.75251(54)	1.8230
10−0	21236.6059(19)	1.74963(42)	1.8739	21234.6338(13)	1.72780(37)	1.8306
11−0	21270.4210(13)	1.75086(48)	1.8817	21268.3950(21)	1.73306(57)	1.8382

[a] Fixed to the value derived from the Dunham coefficients of the 2 $^1\Pi_u$ state, $-\{Y_{02} + Y_{12}(v' + {}^1/_2)\}$, in ref 4.

tion than the deviations in the Dunham-type global fit. To reveal the perturbation in the 2 $^1\Pi_u$ state, we obtained rotationally resolved spectra of the 2 $^1\Pi_u$ $v' = 0-11 \leftarrow$ X $^1\Sigma_g^+$ $v'' = 0$ bands of $^{85}Rb_2$ and $^{85}Rb^{87}Rb$ and determined the effective (or perturbed) band parameters by rotational line position fits using the standard equation:

$$\nu = \nu_0 + B_{v'}^{\text{eff}} J'(J'+1) - D_{v'}[J'(J'+1)]^2 - \{B_{v''}[J''([J''+1) - D_{v''}[J''(J''+1)]^2\} \quad (1)$$

The rotational and centrifugal distortion constants for the ground state, $B_{v''}$ and $D_{v''}$, were held fixed at the values reported by Seto et al.[1] To extract more accurate information about the effects of perturbations on the rotational constants of the 2 $^1\Pi_u$ state, the upper-state $D_{v'}$ was also held fixed at the values reported by Amiot.[4] For all of the rotational analysis presented in this work, we used the PGOPHER program.[22] The determined effective band parameters of the members of the α progression are listed in Table 1. Figure 3 shows the rotationally resolved spectra and simulations of the 2 $^1\Pi_u$ $v' = 0$ (Figure 3a) and $v' = 7$ (Figure 3b) ← X $^1\Sigma_g^+$ $v'' = 0$ bands and the corresponding residuals ($\nu_{\text{observed}} - \nu_{\text{calculated}}$), to which special attention should be paid (see the insets). The residuals of the fit for the 2 $^1\Pi_u$ $v' = 0 \leftarrow$ X $^1\Sigma_g^+$ $v'' = 0$ band (average error of 0.0063 cm^{-1} for 75 observed lines) are smaller and more randomly scattered than those of the 2 $^1\Pi_u$ $v' = 7 \leftarrow$ X $^1\Sigma_g^+$ $v'' = 0$ band (average error of 0.0162 cm^{-1} for 48 observed lines). The rotational line position fits for the 2 $^1\Pi_u$ $v' \leftarrow$ X $^1\Sigma_g^+$ $v'' = 0$ bands up to $v' = 3$ produce similar randomly scattered residuals. However, the residuals in the fit of the 2 $^1\Pi_u$ $v' = 7 \leftarrow$ X $^1\Sigma_g^+$ $v'' = 0$ band is apparently systematically scattered (positive curvature). For the fits of the 2 $^1\Pi_u$ $v' = 6$ and 8 ← X $^1\Sigma_g^+$ $v'' = 0$ bands, we obtained similar systematically scattered residuals. Figure 4 shows (a) $\Delta G_{v'}$ ($= G_{v'+1} - G_{v'}$) and (b) $B_{v'}^{\text{eff}}$ of the 2 $^1\Pi_u$ state versus v'. The $B_{v'}^{\text{eff}}$ values are compared with $B_{v'}$'s of $^{85}Rb_2$ calculated from the Dunham coefficients of the 2 $^1\Pi_u$ state reported in ref 4 and with extrapolated values derived from $v' = 0-3$, which appear to be unperturbed. The $\Delta G_{v'}$ and $B_{v'}^{\text{eff}}$ values show highly irregular behavior, particularly for the $v' > 4$ levels. We found that the 2 $^1\Pi_u$ $v' = 6-8$ levels are shifted to the blue, and the corresponding $B_{v'}^{\text{eff}}$ values are significantly smaller than the expected values. The magnitude of the vibrational level shift is particularly large for the $v' = 7$ and 8 levels. These irregularities of the effective band parameters are clearly correlated with the observed intensities of the red-side extra bands in Figure 2 and indicate that

(i) the 2 $^1\Pi_u$ $v' = 5-8$ levels are significantly perturbed by the red-side perturbers and

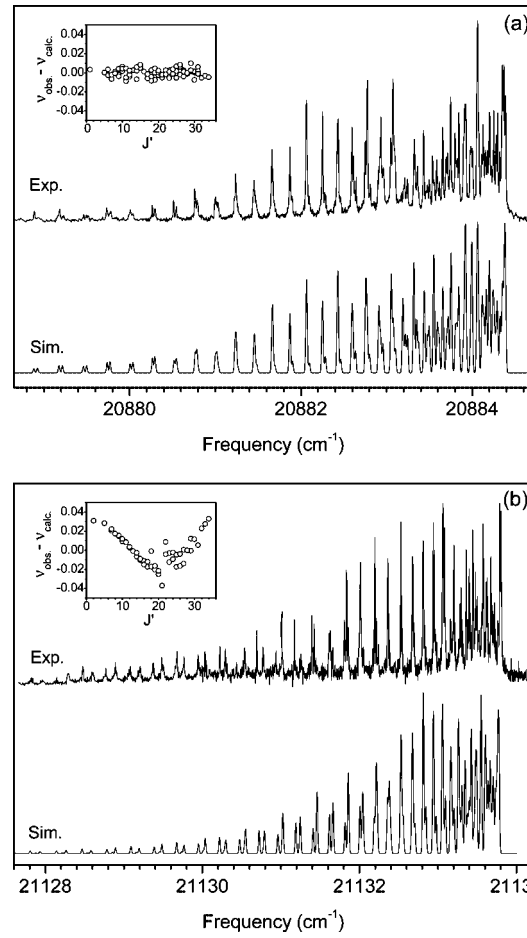

Figure 3. Rotationally resolved spectra and simulations of the 2 $^1\Pi_u$ $v' = 0$ (a) and $v' = 7$ (b) ← X $^1\Sigma_g^+$ $v'' = 0$ bands. The insets show the corresponding residuals of the rotational line position fits. The molecular beam was expanded with 250 Torr of Ar. In the simulations, we set the line width to 0.02 cm^{-1} (Gaussian) and $T_{\text{rot}} = 6.6$ K.

(ii) the rotational constants of the perturbers are smaller than those of the 2 $^1\Pi_u$ v' levels.

The perturber states that lie roughly 6−8 cm^{-1} below the levels of the 2 $^1\Pi_u$ state have rotational levels that are more closely spaced than those of the 2 $^1\Pi_u$ state. As a result, the separation between the corresponding J levels in the perturber state and the 2 $^1\Pi_u$ state increases as a function of J. This causes the lower J levels of the 2 $^1\Pi_u$ state to be more strongly affected by the perturbation than the higher J levels. As a result of the J-dependence of this interaction, the effective rotational constant

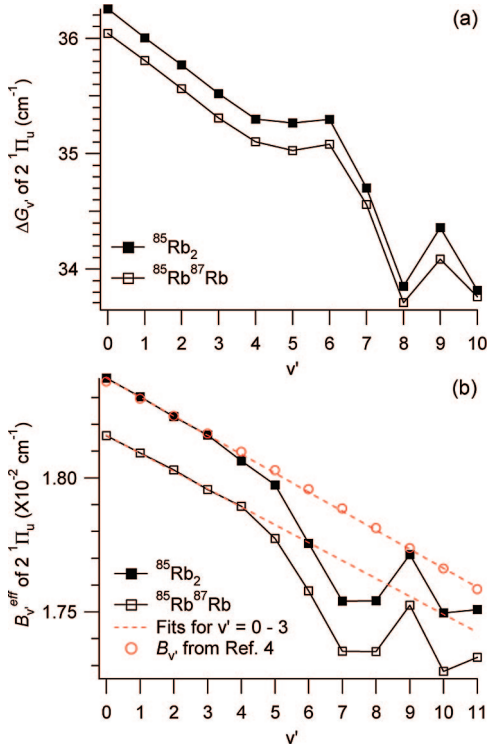

Figure 4. Plots of (a) vibrational spacing, $\Delta G_{v'}$, and (b) effective rotational constants, $B_{v'}^{eff}$ of $^{85}Rb_2$ and $^{85}Rb^{87}Rb$ for the α progression. In (b), red dashed lines are fits for $B_{v'=0-3}^{eff}$ of $^{85}Rb_2$ and $^{85}Rb^{87}Rb$ extrapolated to $v' = 11$, and red circles represents the rotational constants of $^{85}Rb_2$ in the 2 $^1\Pi_u$ state calculated from the Dunham coefficients reported in ref 4.

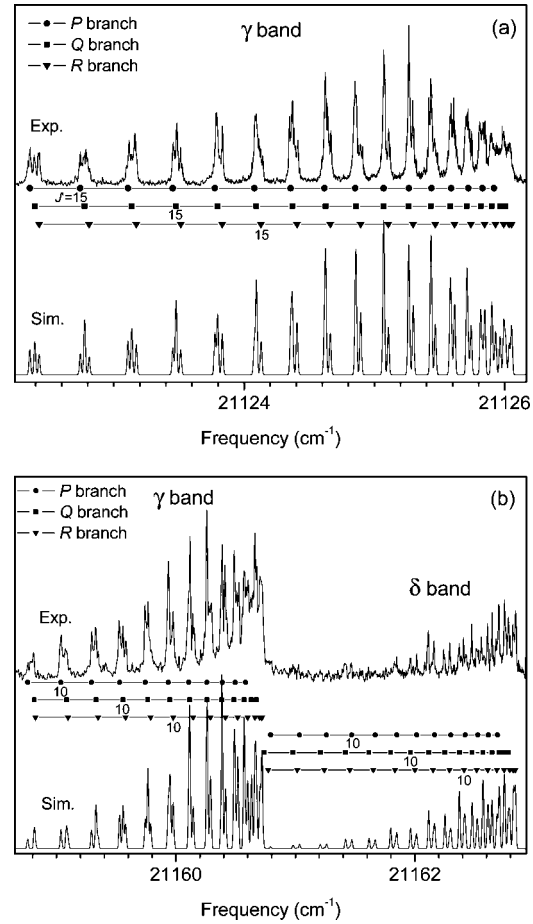

Figure 5. Rotationally resolved spectra of (a) γ band at 21126 cm^{-1} and (b) γ and δ bands near 21162 cm^{-1} and the corresponding simulations generated from the molecular parameters in Table 2. The molecular beam was expanded with (a) 250 and (b) 500 Torr of Ar. In the simulations, we set the line width to 0.02 cm^{-1} (Gaussian) and T_{rot} = (a) 5 and (b) 1.7 K.

of the perturbed 2 $^1\Pi_u$ vibrational levels, is reduced. At the same time, the effective band origin is shifted to higher energies, resulting in an unexpected dependence of $\Delta G_{v'}$ on v'. These effects are clearly observed in Figure 4a,b. The systematic reduction of the effective rotational constants for the $v' = 5-8$, 10, and 11 levels of the 2 $^1\Pi_u$ state from their expected values reflects their perturbation from below by a level with a smaller rotational constant.

3.3. Assignments and Intensity Borrowing Mechanisms of the Perturbing States. Figure 5a,b shows the rotationally resolved spectrum of the γ band at 21126 cm^{-1} and those of the γ and δ bands around 21162 cm^{-1}, respectively, and compares the experimental spectra with the corresponding simulations generated from the band parameters obtained by the following rotational line position fits. The effective band parameters of γ and δ bands listed in Table 2 were determined by rotational line position fits using the following equation:

$$\nu = \nu_0 + (B_{v'}^{eff} \pm q_{v'}/2)J'(J'+1) - \{B_{v''}J''(J''+1) - D_{v''}[J''(J''+1)]^2\} \quad (2)$$

The inclusion of $q_{v'}$, a Λ-doubling parameter, is found to be effective in fitting the γ bands. The (+) and (−) signs of $q_{v'}/2$ in the above equation are for the e- and f-parity rotational levels in the upper vibronic states of γ bands. The ground-state constants, $B_{v''}$ and $D_{v''}$, were held fixed at the values reported by Seto et al.[1] The rotational structures of all γ and δ bands consist of *P*-, *Q*-, and *R*-branch rotational lines, as indicated in Figure 5a,b. This confirms the electronic symmetry of the upper electronic states ($\Omega = 1$), allowing the perturbation with the 2 $^1\Pi_u$ state via spin−orbit coupling ($\Delta\Omega = 0$ with $\Delta J = 0$). The most remarkable difference between the γ and δ bands is found

TABLE 2: Band Parameters of γ and δ Bands (Units in cm^{-1})

	ν_0	$B_{v'}^{eff}$	$q_{v'}$
γ	21056.6518(30)	0.011883(20)	$-1.80(13) \times 10^{-4}$
	21091.2553(20)	0.011570(11)	$-1.40(12) \times 10^{-4}$
	21126.0278(20)	0.011709(8)	$-7.83(89) \times 10^{-5}$
	21160.6959(10)	0.011914(12)	$-2.59(13) \times 10^{-4}$
δ	21162.7966(13)	0.014807(10)	

in their $B_{v'}^{eff}$ values. The $B_{v'}^{eff}$ value of the δ band (0.0148 cm^{-1}) is about 30% larger than those of the γ bands (∼0.0118 cm^{-1}). Figure 6 compares the determined $B_{v'}^{eff}$ values of the γ and δ bands with the corresponding values calculated from the ab initio potential energy curves[16] of the 3 $^3\Sigma_u^+$ and 2 $^3\Pi_u$ states using the LEVEL 7.7 program.[23] For the 2 $^3\Pi_u$ state, the molecular constants were determined previously from the direct observation of the $v' = 0-12$ levels between 19750 and 20300 cm^{-1} by an RE2PI study.[6] In Figure 6, the extrapolated $B_{v'}$ values of the 2 $^3\Pi_u$ state, derived from the low vibrational levels are also shown. From the comparison shown in Figure 6, the upper electronic states of γ and δ bands are assigned to the 3 $^3\Sigma_u^+(1_u)$ and 2 $^3\Pi_u(1_u)$ states, respectively.

Another piece of supporting evidence for the assignments of the extra bands is the isotope shift observed in our mass-resolved RE2PI spectra. Typically, the isotope shift, $\Delta T_{v'} = \omega_e(1-\rho)(v' + {}^1/_2) - \omega_e x_e(1-\rho^2)(v'+{}^1/_2)^2 + \ldots$, in normal potential energy curves increases as the vibrational level goes higher. Figure 7

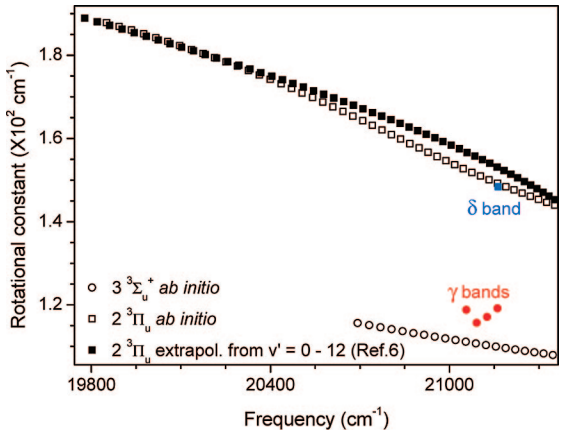

Figure 6. Plot of $B_{v'}^{eff}$'s of γ and δ bands, $B_{v'}$'s calculated using ab initio potential energy curves of the 3 $^3\Sigma_u^+$ and 2 $^3\Pi_u$ states in ref 16, and $B_{v'}$'s of the 2 $^3\Pi_u$ state extrapolated from $B_{v'=0-12}$.

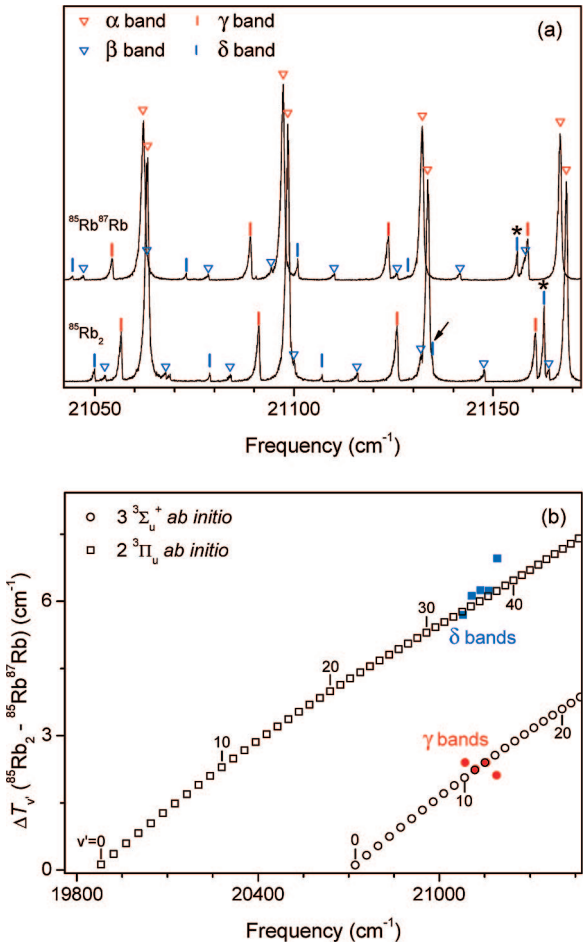

Figure 7. (a) Low-resolution RE2PI spectra of $^{85}Rb_2$ and $^{85}Rb^{87}Rb$ between 21040 and 21170 cm^{-1} recorded with high dye laser intensity (10 times greater than that for the spectrum shown in Figure 2). The arrow indicates the δ band at 21135 cm^{-1}. (b) Isotope shifts between $^{85}Rb_2$ and $^{85}Rb^{87}Rb$ of the γ and δ bands, compared to those calculated using ab initio potential energy curves in ref 16.

shows (a) the RE2PI spectra of $^{85}Rb_2$ and $^{85}Rb^{87}Rb$ obtained with ten times higher laser intensity than that for recording the spectra shown in Figure 2 and (b) the observed isotope shifts, $\Delta T_{v'}$, defined as $T_{v'}$ ($^{85}Rb_2$) − $T_{v'}$ ($^{85}Rb^{87}Rb$), of the γ and δ bands. With increased laser intensity, strong α (indicated by red "▽" for $v' = 5-8$ in Figure 7a) and γ bands were severely saturated and weaker bands could be clearly detected. The γ and δ bands are indicated by red and blue sticks in Figure 7a, respectively. Most of the remaining bands in the spectra indicated by blue "▽" in Figure 7a could be assigned to the β progression, which has small vibrational spacings and strongly red-shaded rotational band contours due to the broad potential well of the 2 $^1\Sigma_u^+$ state, which extends to large internuclear distances. As shown in Figure 7b, the isotope shifts of the δ bands (~6 cm^{-1}) are larger than those of the γ bands (~2 cm^{-1}). Figure 7b compares the observed $\Delta T_{v'}$'s of the γ and δ bands with the calculated values using ab initio potential energy curves of the 3 $^3\Sigma_u^+$ and 2 $^3\Pi_u$ states.[16,23] Ab initio calculations predicted the electronic term values, T_e's, of the 3 $^3\Sigma_u^+$ (20705 cm^{-1}) and 2 $^3\Pi_u$ (19862 cm^{-1}) states.[16] For the 2 $^3\Pi_u$ state, T_e was experimentally determined to be 19875.74(1) cm^{-1}.[6] The v' values of the observed δ bands seem to be around 30−40 of the 2 $^3\Pi_u$ state, based on a comparison of the observed $\Delta T_{v'}$'s and the estimated values from the ab initio calculation.[16] For the γ band at 21067 cm^{-1}, similar comparison of $\Delta T_{v'}$'s suggests that the upper vibronic level is probably the 3 $^3\Sigma_u^+$ $v' = 10$ level.[16] This is consistent with our assignments of the upper electronic states of γ and δ bands to the 3 $^3\Sigma_u^+$ state with higher T_e and the 2 $^3\Pi_u$ state with lower T_e, respectively.

Both the 3 $^3\Sigma_u^+(1_u)$ and 2 $^3\Pi_u(1_u)$ states can borrow transition moments from the bright 2 $^1\Pi_u$ state via spin−orbit coupling ($\Delta\Omega = 0$). The borrowed transition moment of the dark states can be expressed as

$$\begin{aligned}&\langle \text{Dark}, v'_{\text{dark}}|\mu|X^1\Sigma_g^+, v''=0\rangle \\ &= \frac{\langle \text{Dark}, v'_{\text{dark}}|H^{SO}|\text{Bright}, v'_{\text{bright}}\rangle\langle \text{Bright}, v'_{\text{bright}}|\mu|X^1\Sigma_g^+, v''=0\rangle}{E(\text{Dark}, v'_{\text{dark}}) - E(\text{Bright}, v'_{\text{bright}})} \\ &= \langle \text{Dark}|H^{SO}|\text{Bright}\rangle\langle \text{Bright}|\mu|X^1\Sigma_g^+\rangle \times \\ &\qquad \frac{\langle v'_{\text{dark}}|v'_{\text{bright}}\rangle\langle v'_{\text{bright}}|v''=0\rangle}{E(\text{Dark}, v'_{\text{dark}}) - E(\text{Bright}, v'_{\text{bright}})} \quad (3)\end{aligned}$$

The observed vibronic-band intensity distributions of γ and δ progressions are quite different, as shown in both Figures 2 and 7a. This suggests that the intensity borrowing of γ and δ bands is facilitated in different ways, either through Franck−Condon overlap between dark and bright states, $\langle v'_{\text{dark}}|v'_{\text{bright}}\rangle$ or through the energy-level proximity effect, $1/[E(\text{Dark}, v'_{\text{dark}}) - E(\text{Bright}, v'_{\text{bright}})]$.

Let us investigate the intensity borrowing mechanism of the 3 $^3\Sigma_u^+ \leftarrow X\ ^1\Sigma_g^+$ transitions first. When the theoretical T_e value of the 2 $^1\Pi_u$ state (21301 cm^{-1})[16] is reduced by 406 cm^{-1} in comparison with the experimental value (20895 cm^{-1})[4] (compare the ab initio and RKR potential curves of the 2 $^1\Pi_u$ state shown in Figure 1), the 2 $^1\Pi_u$−3 $^3\Sigma_u^+$ potential crossing point is located at 21125 cm^{-1}. The particularly large discrepancy between the theoretical and experimental T_e values of the 2 $^1\Pi_u$ state was mentioned by the authors of ref 16. The crossing point corresponds to the spectral region where the γ bands are observed strongly. This 2 $^1\Pi_u$−3 $^3\Sigma_u^+$ potential curve crossing explains the observed intensities of γ bands well. In this case, several vibrational levels of the 3 $^3\Sigma_u^+(1_u)$ state near the crossing point can borrow spectral intensities from the nearby 2 $^1\Pi_u$ v' levels by the favorable Franck−Condon overlaps.

For the 2 $^3\Pi_u(1_u) \leftarrow X\ ^1\Sigma_g^+$ transitions, the two vibronic bands denoted by "∗" in Figure 7a, which are close to γ bands, are prominent; other vibronic bands, including those close to α bands, are much weaker. From this observation, the energy-level proximity effect between the 3 $^3\Sigma_u^+(1_u)$ and 2 $^3\Pi_u(1_u)$ states can be suggested for the explanation of the observed

intensity distribution of the δ bands. Probably, much of the spectral intensities of the strong δ bands noted by "$*$" are borrowed through the indirect route of 2 $^1\Pi_u \rightarrow 3\ ^3\Sigma_u^+(1_u) \rightarrow 2\ ^3\Pi_u(1_u)$, which is facilitated by the vibronic-level proximity effect between the 3 $^3\Sigma_u^+(1_u)$ and 2 $^3\Pi_u(1_u)$ states.

The spin−orbit interaction terms among the upper vibronic levels of the α, γ, and δ bands and the deperturbed band parameters can be estimated by a deperturbation fit. The interaction terms are expressed as

$$H_{\alpha\gamma} = \langle 2^1\Pi_u, v'_\alpha | H_{SO} | 3^3\Sigma_u^+, v'_\gamma \rangle$$

$$H_{\gamma\delta} = \langle 3^3\Sigma_u^+, v'_\gamma | H_{SO} | 2^3\Pi_u, v'_\delta \rangle$$

and

$$H_{\alpha\delta} = \langle 2^1\Pi_u, v'_\alpha | H_{SO} | 2^3\Pi_u, v'_\delta \rangle \quad (4)$$

We performed 2 × 2 deperturbation fits for the nearest perturbing $\alpha-\gamma$ band pairs (α ($v' = 5$)$-\gamma$ (at 21057 cm^{-1}), α ($v' = 6$)$-\gamma$ (at 21091 cm^{-1}), and α ($v' = 7$)$-\gamma$ (at 21126 cm^{-1})) and a 3 × 3 deperturbation fit for the close-lying α ($v' = 8$), γ, and δ bands around 21164 cm^{-1}. These deperturbations effectively fit the observed rotational line positions of nearby α, γ, and δ bands using the following Hamiltonian matrix:

$$H = \begin{pmatrix} T_{v'}^{\alpha} + F_{v'}^{\alpha}(J') & H_{\alpha\gamma} & H_{\alpha\delta} \\ H_{\gamma\alpha} & T_{v'}^{\gamma} + F_{v'}^{\gamma}(J') & H_{\gamma\delta} \\ H_{\delta\alpha} & H_{\delta\gamma} & T_{v'}^{\delta} + F_{v'}^{\delta}(J') \end{pmatrix} \quad (5)$$

The terms values in the upper vibronic levels of the α, γ, and δ bands are represented by $T_{v'}^{\alpha} + F_{v'}^{\alpha}(J')$, $T_{v'}^{\gamma} + F_{v'}^{\gamma}(J')$, and $T_{v'}^{\delta} + F_{v'}^{\delta}(J')$, respectively. The observed rotational line positions were converted to the term values by adding the rotational term values in the common lower vibronic level (X $^1\Sigma_g^+$ $v'' = 0$). The ground-state constants, $B_{v''}$ and $D_{v''}$, were given by Seto et al.[1] and also the $D_{v'}$ values of the α bands were fixed at the values listed in Table 1.[4] For the rotational terms in the upper vibronic levels of the γ bands, the Λ-doubling parameter was effectively fitted. Figure 8 compares the effective band parameters with those partially deperturbed by the deperturbation fits. The determined band parameters and interaction terms are listed in Table 3. The interaction term, $H_{\alpha\delta}$, is expected to be insignificant considering poor vibrational overlap integrals between the 2 $^1\Pi_u$ and 2 $^3\Pi_u$ states in the observed spectral region. The vibrational overlap integrals between the 2 $^1\Pi_u$ and 3 $^3\Sigma_u^+$ states, $\langle v'_\alpha | v'_\gamma \rangle$, between the 3 $^3\Sigma_u^+$ and 2 $^3\Pi_u$ states, $\langle v'_\gamma | v'_\delta \rangle$, and between the 2 $^1\Pi_u$ and 2 $^3\Pi_u$ states, $\langle v'_\alpha | v'_\delta \rangle$ were calculated using the RKR (2 $^1\Pi_u$)[4] and ab initio (3 $^3\Sigma_u^+$ and 2 $^3\Pi_u$)[16] potential energy curves (see Supporting Information).[23] According to these calculations, the $\langle v'_\alpha | v'_\delta \rangle$ values are much smaller than the $\langle v'_\alpha | v'_\gamma \rangle$ and $\langle v'_\gamma | v'_\delta \rangle$ values (a factor of 10^{-10} times) around the observed spectral region. These particularly small $\langle v'_\alpha | v'_\delta \rangle$ values are due to cancelation of the vibrational overlap by the oscillation of the vibrational wave functions of the 2 $^3\Pi_u$ state. On the other hand, the vibrational overlap integrals, $\langle v'_\alpha | v'_\gamma \rangle$ and $\langle v'_\gamma | v'_\delta \rangle$, are enhanced by the 2 $^1\Pi_u - 3\ ^3\Sigma_u^+$ potential curve crossing and close proximity of the outer walls of the 3 $^3\Sigma_u^+$ and 2 $^3\Pi_u$ potential energy curves, respectively. Therefore, the interaction term, $H_{\alpha\delta}$, was not included in the 3 × 3 deperturbation fit of the close-lying α, γ, and δ bands around 21164 cm^{-1}. This consistently indicates that the spectral intensity of the δ band comes from the indirect pathway of 2 $^1\Pi_u \rightarrow 3\ ^3\Sigma_u^+(1_u) \rightarrow 2\ ^3\Pi_u(1_u)$. The validity of the deperturbation fits are justified by the following:

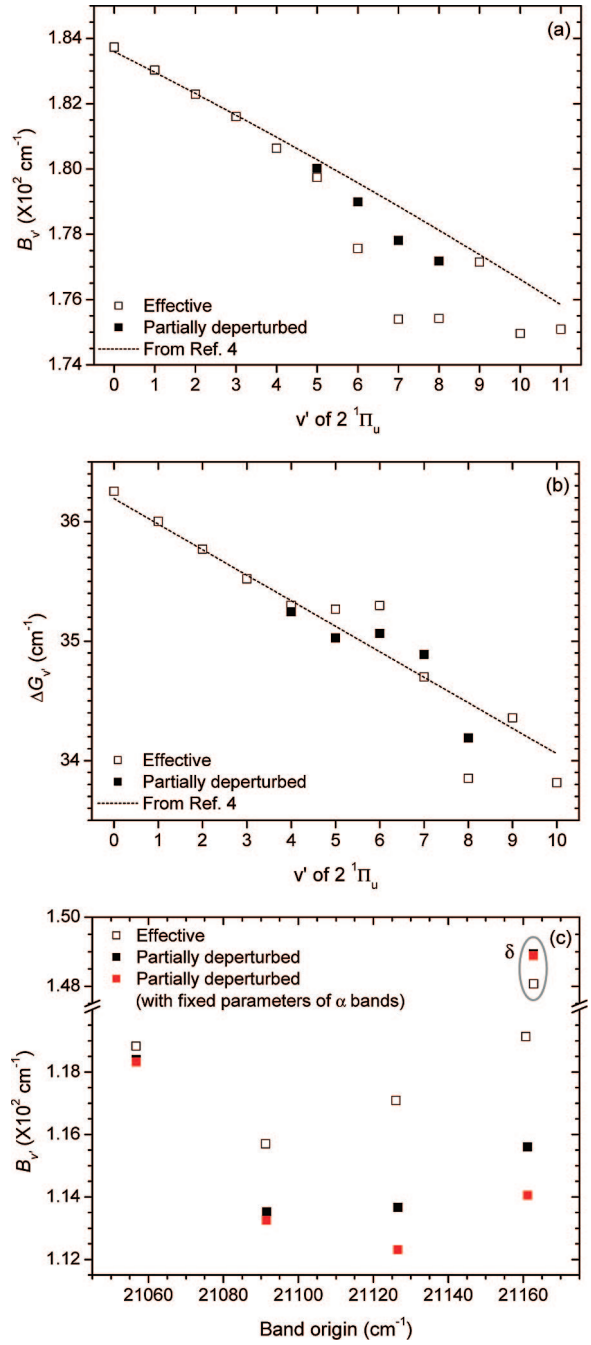

Figure 8. Plots of (a) effective and partially deperturbed $B_{v'}$, (b) effective and partially deperturbed $\Delta G_{v'}$ of the α bands, and (c) effective and partially deperturbed $B_{v'}$ of the γ and δ bands. In (a) and (b) the dashed lines represent the $B_{v'}$ and $\Delta G_{v'}$ values calculated from the Dunham coefficient reported in ref 4, respectively.

(i) The $B_{v'}$ values of the α and γ bands were increased and decreased, respectively, after deperturbations.

(ii) The fluctuations in the $\Delta G_{v'}$ values of the 2 $^1\Pi_u$ state are significantly reduced.

(iii) The $q_{v'}$ values of the γ bands agree with the corresponding value determined by the rotational line position fit of the γ bands in Table 2 within 1Σ level.

The Λ-doubling parameters caused by heterogeneous perturbation are not affected by the spin−orbit coupling. The determined $B_{v'}$ values of the α bands are, however, still smaller than the values derived from the Dunham coefficients of the 2 $^1\Pi_u$ state[4] or the extrapolated values from the unperturbed region of $v' = 0-3$ (see Figure 8a). Also, there are still fluctuations in

TABLE 3: Partially Deperturbed Band Parameters of the α, γ, and δ Bands, and the Interaction Terms through Spin−Orbit Couplings[a]

	ν_0	$10^2 B_{v'}$	$10^4 q_{v'}$	$H_{\alpha\gamma}$	$H_{\gamma\delta}$
$\alpha_{v'=5}$	21063.078(31)	1.8002(16)			
$\gamma_1{}^b$	21056.709(32)	1.1840(38)	−1.80(19)		
$\alpha_{v'=6}$	21098.106(20)	1.7899(11)			
$\gamma_2{}^b$	21091.564(21)	1.1352(18)	−1.38(11)		
$\alpha_{v'=7}$	21133.170(22)	1.7781(11)			
$\gamma_3{}^b$	21126.576(23)	1.1367(17)	−0.96(9)		
$\alpha_{v'=8}$	21168.058(44)	1.7718(23)			
$\gamma_4{}^b$	21161.125(64)	1.156(11)	−2.59(29)		
$\delta_1{}^b$	21162.714(75)	1.4894(95)			
$\alpha_{v'=5}-\gamma_1{}^b$				0.61(17)	
$\alpha_{v'=6}-\gamma_2{}^b$				1.463(48)	
$\alpha_{v'=7}-\gamma_3{}^b$				1.992(39)	
$\alpha_{v'=8}-\gamma_4{}^b$				1.59(11)	
$\gamma_4-\delta_1{}^b$					0.43(17)

[a] The band parameters for the α−γ band pairs, α ($v' = 5$)−γ (at 21057 cm^{-1}), α ($v' = 6$)−γ (at 21091 cm^{-1}), and α ($v' = 7$)−γ (at 21126 cm^{-1}) were determined by 2 × 2 deperturbation and those for the close-lying α ($v' = 8$), γ (at 21161 cm^{-1}), and δ (at 21163 cm^{-1}) bands by 3 × 3 deperturbation. Units are in cm^{-1}. [b] γ_1, γ_2, γ_3, γ_4, and δ_1 represent the γ and δbands at 21057, 21091, 21126, 21161, and 21163 cm^{-1}, respectively.

the $B_{v'}$ values of the γ bands after deperturbation. This implies that the deperturbations have not yet been completed. The additional perturbation may come from the interactions between the upper vibronic levels of the α bands and the second nearest γ bands and between the upper levels of the γ bands and the weak overlapped δ band through spin−orbit coupling. L-uncoupling (or Ω-uncoupling) interactions between the Ω = 1 states (2 $^1\Pi_u$, 3 $^3\Sigma_u{}^+(1_u)$, and 2 $^3\Pi_u(1_u)$) and the Ω = 0 states (2 $^1\Sigma_u{}^+$ and 2 $^3\Pi_u(0_u{}^+)$) can also contribute to overall perturbations. However, the interaction terms between the upper vibronic levels of the α band and the second nearest γ band could not be determined simultaneously. Floating these additional interaction terms shows strong correlation with the band origins of the connected bands. Subsequently, we fixed all the parameters (ν_0, $B_{v'}$, and $D_{v'}$ as well as $B_{v''}$ and $D_{v''}$) of the α bands ($v' = 5-8$). The α-band parameters of the upper vibronic levels are fixed at the values derived from the Dunham coefficients of the 2 $^1\Pi_u$ state. With these restrictions on the band parameters, the interaction terms, $H_{\alpha(v'=5)\gamma(\mathrm{at}21091\mathrm{cm}^{-1})}$, $H_{\alpha(v'=6)\gamma(\mathrm{at}21126\mathrm{cm}^{-1})}$, and $H_{\alpha(v'=7)\gamma(\mathrm{at}21161\mathrm{cm}^{-1})}$, could be obtained. The determined band parameters and interaction terms using this restricted 9 × 9 deperturbation fit, listed in Table 4, agree well with the corresponding values determined by the 2 × 2 and 3 × 3 deperturbation fits. $H_{\alpha(v'=5)\gamma(\mathrm{at}21091\mathrm{cm}^{-1})}$, $H_{\alpha(v'=6)\gamma(\mathrm{at}21126\mathrm{cm}^{-1})}$, and $H_{\alpha(v'=7)\gamma(\mathrm{at}21161\mathrm{cm}^{-1})}$ values appear to be reasonable in comparison with the interaction values of the nearest α-γ band pairs. In Figure 8c, the further deperturbed $B_{v'}$ values of the γ bands are compared with the effective values and those obtained by the 2 × 2 and 3 × 3 deperturbation fits. The remaining fluctuations in the $B_{v'}$ values of the γ bands may arise from the spin−orbit interactions of the upper vibronic levels the γ bands at 21091, 21126, and 21161 cm^{-1} from the nearby 2 $^3\Pi_u(1_u)$ vibronic levels (see Figure 7a). Figure 9 compares the residuals of deperturbation fits for the α bands ($v' = 5-8$) with those of the fits with effective parameters. The systematic dispersions of the residuals, which appears in the fits of the α ($v' = 6-8$) bands with effective parameters, were reduced greatly after the deperturbations. This also validates both the 2 × 2 (and 3 × 3) and restricted 9 × 9 deperturbation fits. From the residuals of the fit for the α ($v' = 7$) band shown in Figure 9c, we could find another feature of perturbation. The behavior of the residuals around $J' = 20-23$ suggests that the rotational energy structure of the 2 $^1\Pi_u$ $v' = 7$ level is crossed by that of another perturber. Probably, the upper vibronic state of the δ band at 21135 cm^{-1}, indicated by the arrow in Figure 7a, is responsible for this rotational energy level crossing.

Finally, we discuss the estimation of the electronic part of the 2 $^1\Pi_u$−3 $^3\Sigma_u{}^+(1_u)$ interaction terms. Assuming that the electronic part of the interaction terms are independent of the internuclear distance, $H_{\alpha\gamma}$ can be represented as follows:

$$H_{\alpha\gamma} = \langle 2^1\Pi_u | H_{SO} | 3^3\Sigma_u^+ \rangle \langle v'_\alpha | v'_\gamma \rangle = H^{el} \langle v'_\alpha | v'_\gamma \rangle \qquad (6)$$

Similarly to the case of K_2 A $^1\Sigma_u{}^+$ and b $^3\Pi_u$ states,[24] we are dealing with near-degenerate vibrational levels of the two crossing potential curves of the 2 $^1\Pi_u$ and 3 $^3\Sigma_u{}^+$ state. Therefore, H^{el} can be factored out from $H_{\alpha\gamma}$ as above and regarded as the value at the potential crossing point $H^{el}(R_c)$ by the *R*-centroid approximation.[21] We could extract the electronic part by employing values of $\langle v'_\alpha | v'_\gamma \rangle$ listed in the Supporting Information. Table 4 shows the H^{el} values extracted from the $H_{\alpha\gamma}$ values obtained by the restricted 9 × 9 deperturbation fit. We assumed the vibrational quantum numbers of the γ bands as 10 − 13 and adopted the corresponding $\langle v'_\alpha | v'_\gamma \rangle$ values. The off-diagonal spin−orbit coupling matrix element between the 2 $^1\Pi_u$ and 3 $^3\Sigma_u{}^+(1_u)$ states at their potential curve crossing point is thus obtained as 118(60) cm^{-1}. The rather large uncertainty in $H^{el}(R_c)$ mainly comes from the uncertainty of $\langle v'_\alpha | v'_\gamma \rangle$. The slope of the inner wall of the 3 $^3\Sigma_u{}^+$ potential energy curve at the crossing point is expected to have critical effect on vibrational overlap. The uncertainty of the suggested $H^{el}(R_c)$ thus depends on the accuracy of the ab initio potential energy curve of the 3 $^3\Sigma_u{}^+$ state. Also, the assumption of v' values of the observed γ bands as 10−13 can introduces additional uncertainty in $H^{el}(R_c)$, although the comparison of the observed isotope shifts of the γ bands with the corresponding calculated values supports this assignment (see Figure 7b). Both the 2 $^1\Pi_u$ and 3 $^3\Sigma_u{}^+(1_u)$ states dissociate into the atomic dissociation limit of Rb(5s) + Rb(4d). However, the small atomic spin−orbit parameter of the Rb 4d ^{2}D term, ζ_{4d} = 0.178 cm^{-1} cannot rationalize the experimentally determined $H^{el}(R_c)$ between the 2 $^1\Pi_u$ and 3 $^3\Sigma_u{}^+(1_u)$ states.[25] According to the ab initio calculation,[14] the inner limb of the adiabatic potential curve of the 3 $^3\Sigma_u{}^+$ state has Rb(5p) atomic character. This is due to the avoided crossing between the repulsive $^3\Sigma_u{}^+$ state dissociating into Rb(5s) + Rb(5p) and another $^3\Sigma_u{}^+$ state. The atomic spin−orbit parameter of the Rb 5p ^{2}P term, ζ_{5p} = 158.400 cm^{-1}, is the largest among those of the Rb atomic terms.[25] Probably, the large off-diagonal spin−orbit coupling matrix element between the 2 $^1\Pi_u$ and 3 $^3\Sigma_u{}^+(1_u)$ states are dominated by the Rb(5p) atomic character of the electronic wave function of the 3 $^3\Sigma_u{}^+(1_u)$ state.

For heavy alkali metal diatomic molecules, information on the off-diagonal spin−orbit coupling matrix elements is particularly important in treating the perturbation and predissociation dynamics in detail. Theoretical calculations for off-diagonal spin−orbit interactions between the electronic states of Rb_2 are, however, rare and limited to those between a few low-lying excited electronic states.[17] Our experimental estimation of the off-diagonal spin−orbit matrix element between the 2 $^1\Pi_u$ and 3 $^3\Sigma_u{}^+(1_u)$ states could become useful for theoretical studies of relativistic effects in Rb_2.

4. Conclusion

We have experimentally observed and assigned the spin-forbidden transitions of 3 $^3\Sigma_u{}^+(1_u)$ and 2 $^3\Pi_u(1_u)$ ← X $^1\Sigma_g{}^+$ in

TABLE 4: Partially Deperturbed Band Parameters of the γ, and δ Bands, and the Interaction Terms through Spin−Orbit Couplings[a]

	ν_0	$10^2 B_{v'}$	$10^4 q_{v'}$	$H_{\alpha\gamma}$	$\langle v'_\alpha \vert v'_\gamma \rangle^c$	H^{eld}	$H_{\gamma\delta}$
$\gamma_1{}^b$	21056.718(10)	1.1833(52)	−1.80(34)				
$\gamma_2{}^b$	21091.500(8)	1.1325(18)	−1.38(19)				
$\gamma_3{}^b$	21126.536(8)	1.1231(14)	−0.99(16)				
$\gamma_4{}^b$	21161.178(6)	1.1406(46)	−2.51(52)				
$\delta_1{}^b$	21162.715(3)	1.4889(22)					
$\alpha_{v'=5}-\gamma_1{}^b$				0.656(33)	3.40×10^{-3}	193	
$\alpha_{v'=6}-\gamma_2{}^b$				1.490(13)	1.58×10^{-2}	94	
$\alpha_{v'=7}-\gamma_3{}^b$				2.2098(88)	3.56×10^{-2}	62	
$\alpha_{v'=8}-\gamma_4{}^b$				1.9588(32)	2.80×10^{-2}	70	
$\gamma_4-\delta_1{}^b$							0.43[e]
$\alpha_{v'=5}-\gamma_2{}^b$				1.446(45)	5.67×10^{-3}	255	
$\alpha_{v'=6}-\gamma_3{}^b$				2.207(24)	2.16×10^{-2}	102	
$\alpha_{v'=7}-\gamma_4{}^b$				1.941(28)	3.75×10^{-2}	51	

[a] Units are in cm^{-1}. Band parameters of the α bands were held fixed at the values reported in ref 4 during the deperturbation fit to reduce the number of floated parameters. [b] γ_1, γ_2, γ_3, γ_4, and δ_1 represent the γ and δ bands at 21057, 21091, 21126, 21161, and 21163 cm^{-1}, respectively. [c] Calculated using the RKR potential energy curve of the 2 $^1\Pi_u$ state (ref 4) and the ab initio potential energy curve of the 3 $^3\Sigma_u{}^+$ state (ref 16). The vibrational quantum numbers of the γ_1, γ_2, γ_3, and γ_4 bands are assumed as 10, 11, 12, and 13, respectively. [d] Electronic part of the interaction term, $H_{\alpha\gamma}$. $H^{el} = H_{\alpha\gamma}/\langle v'_\alpha | v'_\gamma \rangle$. [e] Fixed to the value determined by the 3 × 3 deperturbation fit.

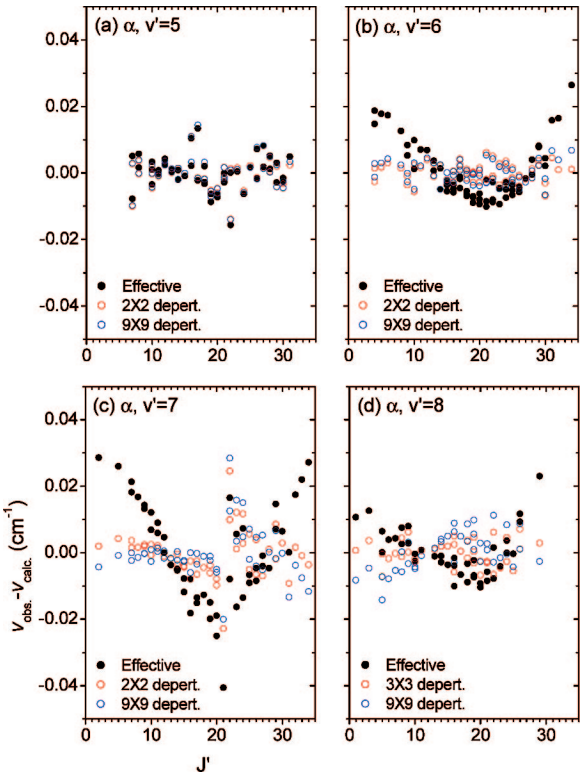

Figure 9. Plots of residuals of fits for (a) the α ($v' = 5$), (b) α ($v' = 6$), (c) α ($v' = 7$), and (d) α ($v' = 8$) bands. The black filled circles represent the residuals of the fits with effective band parameters. The open circles represent the residuals of the 2 × 2 (and 3 × 3) and 9 × 9 deperturbation fits.

the vicinity of the 2 $^1\Pi_u \leftarrow$ X $^1\Sigma_g{}^+$ band system of Rb_2 for the first time. The 3 $^3\Sigma_u{}^+(1_u)$ and 2 $^3\Pi_u(1_u)$ states, which are out of the Franck−Condon region in this spectral region, borrow their transition moments from the 2 $^1\Pi_u$ state. The detailed intensity borrowing mechanisms of the 3 $^3\Sigma_u{}^+(1_u)$ and 2 $^3\Pi_u(1_u) \leftarrow$ X $^1\Sigma_g{}^+$ transitions have been found to be different. The 3 $^3\Sigma_u{}^+ \leftarrow$ X $^1\Sigma_g{}^+$ system is found to be enhanced in the vicinity of the curve crossing between the 3 $^3\Sigma_u{}^+$ state and the 2 $^1\Pi_u$ state, due to spin−orbit mixing of the 1_u components of these states. In contrast, the 2 $^3\Pi_u(1_u) \leftarrow$ X $^1\Sigma_g{}^+$ system is found to be enhanced when levels of the 2 $^3\Pi_u(1_u)$ state lie close to levels of the 3 $^3\Sigma_u{}^+(1_u)$ state. In this case, the vibronic energy level proximity effect shows that the 2 $^3\Pi_u(1_u)$ state borrows intensity from the 3 $^3\Sigma_u{}^+(1_u)$ state, which in turn obtains its intensity from the 2 $^1\Pi_u \leftarrow$ X $^1\Sigma_g{}^+$ system. The off-diagonal spin−orbit coupling matrix element between the 2 $^1\Pi_u$ and 3 $^3\Sigma_u{}^+(1_u)$ states has been estimated as 118(60) cm^{-1}. The large electronic interaction term, probably, is due to the Rb(5p) atomic character of the electronic wave function of the 3 $^3\Sigma_u{}^+(1_u)$ state.

Acknowledgment. This work was partially supported by MEST of Korea through the APRI-Research Program of GIST. We thank KRF for the financial support through ABRL (R14-2005-033-0100) and KOSEF for support through the Center for Intelligent NanoBio Materials (Grant R11-2005-008-00000-0). S.L. thanks KRF for financial support (KRF-2006-311-C00078) and KISTI supercomputing center (KSC-2007-S00-1028). We are grateful to Dr. Colin M. Western and Prof. Jin-Tae Kim for many helpful discussions.

Supporting Information Available: Analysis of the rotationally resolved RE2PI spectrum of $^{85}Rb_2$ at 21294 cm^{-1}. Vibrational overlap integrals between the 2 $^1\Pi_u$ state and the 3 $^3\Sigma_u{}^+$ state, between the 3 $^3\Sigma_u{}^+$ state and the 2 $^3\Pi_u$ state, and between the 2 $^1\Pi_u$ state and the 2 $^3\Pi_u$ state. This information is available free of charge via the Internet at http://pubs.acs.org.

References and Notes

(1) Seto, J. Y.; Le Roy, R. J.; Vergès, J.; Amiot, C. *J. Chem. Phys.* **2000**, *113*, 3067.
(2) Amiot, C. *Mol. Phys.* **1986**, *58*, 667.
(3) Amiot, C.; Vergès, J. *Mol. Phys.* **1987**, *61*, 51.
(4) Amiot, C. *J. Chem. Phys.* **1990**, *93*, 8591.
(5) Tsi-Zé, N.; San-Tsiang, T. *Phys. Rev.* **1937**, *52*, 91.
(6) Lee, Y.; Yoon, Y.; Baek, S. J.; Joo, D.-L.; Ryu, J.; Kim, B. *J. Chem. Phys.* **2000**, *113*, 2116.
(7) Yoon, Y.; Lee, Y.; Lee, S.; Kim, B. *J. Chem. Phys.* **2002**, *116*, 6660.
(8) Lee, Y.; Lee, S.; Kim, B. *J. Phys. Chem. A* **2007**, *111*, 1750.
(9) Breford, E. J.; Engelke, F. *Chem. Phys. Lett.* **1980**, *75*, 132.
(10) Zhang, B.; Berg, L.-E.; Hansson, T. *Chem. Phys. Lett.* **2000**, *325*, 577.
(11) Gador, N.; Zhang, B.; Andersson, R.; Johansson, P.; Hansson, T. *Chem. Phys. Lett.* **2003**, *368*, 202.
(12) Tsai, C. C.; Freeland, R. S.; Vogels, J. M.; Boesten, H. M. J. M.; Verhaar, B. J.; Heinzen, D. J. *Phys. Rev. Lett.* **1997**, *79*, 1245.
(13) Shapiro, E. A.; Shapiro, M.; Pe'er, A.; Ye, J. *Phys. Rev. A* **2007**, *75*, 013405.
(14) Spiegelmann, F.; Pavolini, D.; Daudey, J. P. *J. Phys. B: At. Mol. Phys.* **1989**, *22*, 2465.

(15) Foucrault, M; Millie, Ph; Daudey, J. P *J. Chem. Phys.* **1992**, *96*, 1257.

(16) Park, S. J.; Suh, S. W.; Lee, Y. S.; Jeung, G.-H. *J. Mol. Spectrosc.* **2001**, *207*, 129.

(17) Edvardsson, D.; Lunell, S.; Marian, C. M. *Mol. Phys.* **2003**, *101*, 2381.

(18) Gerstenkorn, S.; Luc, P. *Atlas du Spectre d'Absorption de la Molécule d'Iode Entre 14800−20000 cm*$^{-1}$; CNRS: Paris, 1978.

(19) Clouthier, D. J.; Karolczak, J. *Rev. Sci. Instrum.* **1990**, *61*, 1607.

(20) Hammond, C. J.; Reid, K. L.; Ronayne, K. L. *J. Chem. Phys.* **2006**, *124*, 201102.

(21) Lefebvre-Brion, H.; Field, R. W. *The Spectra and Dynamics of Diatomic Molecules*; Elsevier; New York, 2004.

(22) Western, C. M. *PGOPHER version 5.2, a Program for Simulating Rotational Structure*; University of Bristol: Bristol, U.K., 2007 (http://pgopher.chm.bris.ac.uk).

(23) Le Roy, R. J. *LEVEL 7.7. A Computer Program for Solving the Radial Schrödinger Equation for Bound and Quasibound Levels* ; University of Waterloo Chemical Physics Research Report CP-661; University of Waterloo: Waterloo, ON, CA, 2005.

(24) Jong, G.; Li, L.; Whang, T.-J.; Stwalley, W. C.; Coxon, J. A.; Li, M.; Lyyra, A. M. *J. Mol. Spectrosc.* **1992**, *155*, 115.

(25) Sansonetti, J. E. *J. Phys. Chem. Ref. Data* **2006**, *35* (1), 301.

JP801560A